Trans. JSASS Aerospace Tech. Japan
Vol. 14, No. ists30, pp. Pf_51-Pf_60, 2016

Finite Element Analysis of Vibration Amplification Distribution in Lean Satellites

By Amgalanbat BATSUREN, Toru HATAMURA, Hirokazu MASUI and Mengu CHO

Kyushu Institute of Technology, Kitakyushu, Japan

(Received July 31st, 2015)

This paper presents a part of the basic research for establishing the unit Qualification Test (QT) conditions within the framework of an international project to make ISO standard, namely, "Space Systems—Design Qualification and Acceptance Tests for Small-Scale Satellites and Units Requiring Low Costs and Fast Delivery". A laboratory test is conducted to study how vibration acceleration is distributed in a satellite body, so as to define the unit QT random vibration test level. The range of natural frequency and the amplification of acceleration are identified through statistical analysis of the test results. Finite element analysis is carried out to extend the findings to other structural types of micro/nanosatellites. Three structural types are analyzed, i.e., Yojo han, T-type and Pi-type. Based on the results, a unit QT vibration level that provides the minimum reliability assurance for use in space is proposed.

Key Words: Finite Element Analysis, Small Satellites, Random Vibration Test, International Standards

Nomenclature

AT	:	acceptance test
DM	:	dummy mass
γ	:	confidence coefficient
k	:	normal tolerance factor
NTL	:	normal tolerance limit
n	:	sample number
OBC	:	onboard computer
PAF	:	payload adapter fitting
PCU	:	power control unit
PSD	:	power spectrum density
Q	:	Q factor
QT	:	qualification test
RF	:	radio frequency unit
s_y	:	standard deviation

1. Introduction

To date, existing environmental test standards are only applicable to large- and medium-sized satellites that demand very high reliability. Those standards are not suitable for micro/nanosatellites, which try to achieve both low cost and fast delivery by making use of Commercial-Off-The-Shelf (COTS) units that do not qualify for use in space. The mission success rate of micro/nanosatellites is, however, much lower than that of large/medium satellites that employ a traditional development style and use space-qualified units.[1)] However, adopting testing standards for traditional satellites would weaken the low-cost, fast-delivery advantage of micro/nanosatellites. There is a need for testing standards suitable for micro/nanosatellites, to improve reliability while maintaining the low-cost, fast-delivery benefit.

In 2011, a project called "Nanosatellite Environment Test Standardization" (NETS) was initiated with the support of Japanese government funding.[2)] The project has been promoted by four institutions, i.e., the Kyushu Institute of Technology, the International Standard Innovation Technology Research Association, the Society of Japanese Aerospace Companies, and Astrex, along with the participation of domestic and international stakeholders. The goal of the project is to establish an ISO standard including an environmental test for micro/nanosatellite systems and units. As of September 2014, a document entitled "Space Systems—Design Qualification and Acceptance Tests of Small-Scale Satellites and Units Requiring Low Cost and Fast Delivery" is being circulated as a committee draft (ISO/CD/19683). The satellites dealt with in ISO/CD/19683 are primarily composed of non-space-qualified COTS units for the achievement of low costs and fast delivery. Their mass and size are, but are not limited to, typically less than 50 kg and 50 cm, respectively. The present paper deals with a vibration test to qualify a unit.

To achieve fast delivery, micro/nanosatellites are often built by integrating units purchased from the market with only the key units developed in-house, unless education/training is the main purpose of the satellite program. At present, there are many COTS units available on the market; some are even sold via the Internet. However, those units often lack test histories under which they are qualified for space use. Therefore, the buyers, i.e., satellite developers, are reluctant to purchase the units and may turn to a product built by manufactures with traditional design/procurement/manufacturing/testing practices. If a COTS product has already passed a certain level of testing defined by a reliable standard, the satellite developer can choose such units with greater confidence. One aim in defining a standard is to define the qualification test (QT) level a unit has to pass before being sold as a product for use in space.

For a unit QT, ISO/CD/19683 is meant to provide a

minimum guarantee that a given unit sold as "a satellite unit" has a certain level of tolerance against the space environment. Therefore, the unit QT under ISO/CD/19683 does not include a proper margin against the maximum predicted environmental stress, which differs/varies from satellite to satellite. A standard provides numeric values for the test level and duration of unit QTs, as much as possible with the rationale of the numeric values given in its annex. If the unit manufacturers adopt this standard, they will carry out the QT according to the testing requirements as part of their qualification process. Then they can add value to their product when they sell it as "a satellite unit" on the market. The basic point is that the unit manufacturer would not develop a custom-made product; the satellite developers would select units from the inventory that best fit their needs. The unit manufacturer would provide the QT report upon request. The satellite developers might then carry out another QT using a dedicated test model. Note that as long as the unit uses COTS parts, there is a little guarantee that the test model is the same as the flight model. Satellite developers might carry out a proto-flight-test (PFT) using a flight model or only an acceptance test (AT), taking the risk of little safety margin. There may be other options, but the important point is that the satellite developers will make consistent decisions about how to obtain the safety margin. They would be responsible for the decision. They would provide the test levels and duration of the additional QT, AT or PFT.

The purpose of the present research is to develop a basis for the unit QT level of random vibration test in ISO/CD/19683. For traditional satellite units, the random vibration test level is derived by taking into account various safety margins (see Ref. [3] for an example). For micro/nanosatellite testing, no margin is included.

A series of random vibration tests using a 50-kg- and 50-cm-class microsatellite were used to derive the unit QT level for ISO/CD/19683. The results are described in Refs. 4) and 5). We investigated the resonant frequency, the Amplification Factor (AF) of each accelerometer mounted at different points inside the satellite, and calculated the resonant frequencies and the maximum AF. Statistically estimating the interval of the resonant frequency range, we derived normal tolerance limits (NTL) for the AF.

In addition to the experiment carried out in-house, vibration test data of seven 50-kg-class microsatellites were collected.[6)] Although the data gave only the measurement at the top corner of the satellites, it was enough to estimate the resonance of the internal points at low frequencies (20 to 300 Hz), as the internal structure is affected by the resonance of the overall satellite structure. The collected data were analyzed to derive statistics at lower frequencies, in the range of 20 to 300 Hz. The unit QT level was derived and then proposed at an expert meeting in November 2013. The proposed level is shown by a solid curve without marks in Fig. 1. At the meeting, it was decided to smooth out the jaggy PSD, as it was difficult for a shaker controller to adopt. Finally the lines marked in circles in Fig. 1 were adapted and included in the draft of ISO/CD/19683

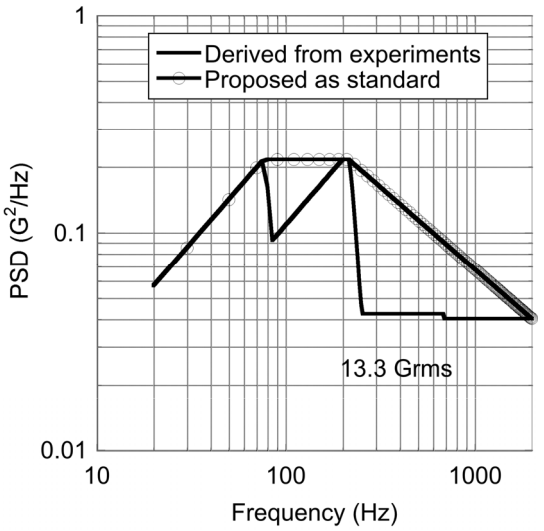

Fig. 1. Unit QT random vibration level derived from the experimental study (without marks) and the test level adopted by ISO/CD/19683 (with circles).

The purpose of the present paper is to extrapolate from and extend these experimental results by Finite Element (FE) analysis. Laboratory testing can be done to investigate the vibration acceleration distribution of various small satellite structures, but they are commonly complex and very expensive. FE analysis of the vibration acceleration distribution allows us to extrapolate from our findings without using expensive laboratory tests for other typical micro/nanosatellite structures.

This paper is composed of five parts. The second part describes the accuracy of the analysis. The third part describes the analysis. The fourth part discusses the unit QT level to be used in the standard. The fifth part gives an overall conclusion and explains the direction of our future work.

2. Verification of Finite Element Analysis

Before we extrapolate from the experimental findings to various types of satellite structures, we need to verify that the analysis is correct. We first compared the FE analysis with our experimental results. In the experiment, we used a dummy satellite, shown in Fig. 2, to obtain the acceleration distribution inside the satellites.

The dummy satellite comprised of basic satellite functions, such as an RF transmitter (0.62kg), a PCU (2.23 kg), a battery (2.21kg) and a computer (0.92kg) (see Ref. 4 for details). The other units were made as dummy mass with a heater inside the units. There were 10 identical dummy masses, each weighing 2.22 kg, and one heavy mass (5.12 kg) inside the central core. The satellite was fixed to the vibration machine using a mock-up of a payload adaptor fitting (PAF) and a jig. The dummy satellite was structurally similar to the so-called Yojo-han type. "Yojo-han" refers to the layout pattern of traditional Japanese tatami mats. When internal structure of the satellite is viewed from above, the lines resemble the tatami layout pattern.

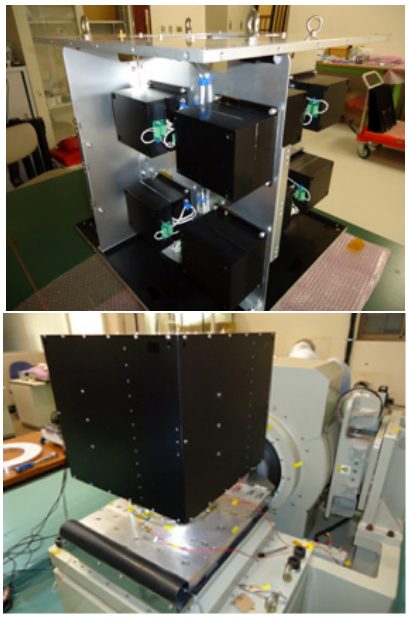

Fig. 2. Internal panel [TOP] and external view [BOTTOM] of dummy satellite.

Figure 3 shows some of the accelerometer positions. The accelerometers were attached to the internal panels of the satellite rather than the unit boxes. Accelerometers were attached to all 10 identical dummy masses (2.22 kg), labelled from DM1 to DM10, but not attached to the heavy one (5.12 kg) in the central core. Base accelerometers were mounted on a jig to calculate the AF. Vibration tests were performed along the X, Y and Z satellite axes.

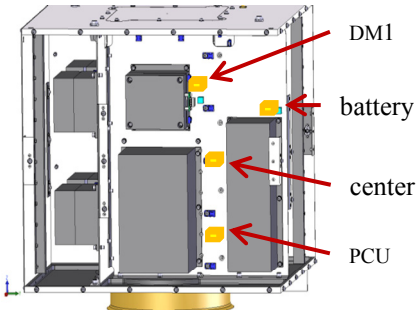

Fig. 3. Layout of accelerometers (yellow boxes indicate accelerometers).

For FE analysis, Nei-Nastran® version 10.1 was used. Among the four linear solvers (PCGLSS, PSS, VSS and VIS) included in the Nastran, we used the PSS solver, which is a fast parallel direct solver and is highly scalable for multiple CPUs/core processors. FEMAP® version 11, which was tightly integrated with the NEi Nastran solver, was used for pre- and post-processing.

The satellite models were created using beam and plate elements. These elements are suitable for the linear dynamic analysis. The material and property were defined for the meshing process for the internal and external panels. We defined the material by selecting a standard material from the Femap material library. The solid model was created with a mesh size of 10 mm on the internal panels of the satellite structure. A finite element model of the dummy satellite used in the FE analysis was constructed, as shown in Fig. 4. The total number of elements and nodes of the dummy satellite finite element model were 48,381 and 80,051, respectively. The panel thickness was set to 2mm for the internal panels and 1.5mm for the external panels. We used a model of a real jig that was used for the experiment. The jig also represented PAF. It was meshed using eight-node hexahedral solid mesh, as shown in Fig. 5. This meshing resulted in approximately 24,684 tetrahedral solid elements. The analyzed satellite model was made of aluminum with aluminum alloy AL5052, while the jig and adaptor are made of AL2024.

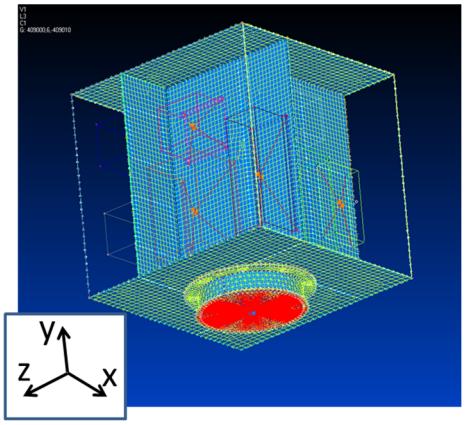

Fig. 4. Finite element model of the dummy satellite.

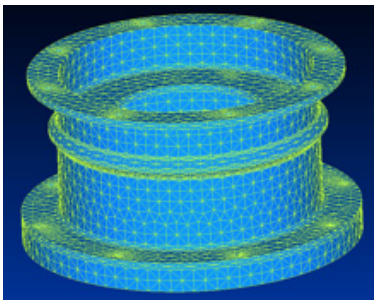

Fig. 5. Finite element model of the jig.

In the analysis, the satellite and jig/adaptor were connected by bar elements. The jig in Fig. 5 is attached to the bottom of satellite. Figure 4 shows the satellite and jig (PAF) already attached. The jig (PAF) was connected to the satellite by eight bolts. These bolts were not exactly modeled but were modeled by “bar elements”. At other locations, the satellite and the jig (PAF) were attached, though without any binding force.

A single node was selected as a virtual sensor near the unit. In total, 18 virtual sensors were used to collect vibration acceleration responses at different positions on the internal panels of the dummy satellite. The virtual sensor positions were exactly the same for both the experiment and the analysis of the dummy satellite. Figure 6 shows an example of

the virtual sensor positions. The black circles indicate the position of virtual sensors.

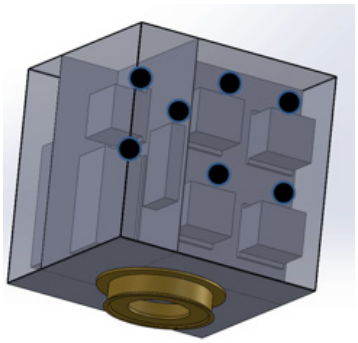

Fig. 6. Dummy satellite virtual sensor position.

Random vibration loads are directly applied to the cylinder-shaped jig in the x, y, z directions. We used a low-level input load in order to avoid nonlinear material behavior. Figure 7 shows the Power Spectral Density (PSD) applied to the base.

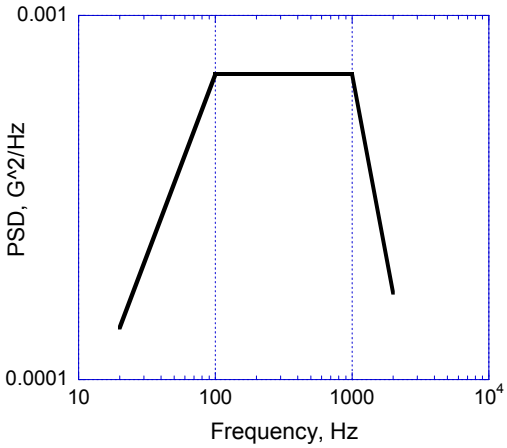

Fig. 7. The base level vibration PSD.

Comparisons between analysis and experiments are shown in Tables 1, 2 and 3. In the table, AF means the amplification factor, which is defined as the square root of the ratio of the measured PSD value at a given point by the base level. The data listed in Tables 1, 2 and 3 correspond to the case when the excitation was given in the x-direction.

Figure 8 illustrates the best agreement in quantitative comparison. At the first stage, the results of analysis were not in good agreement with the experimental data results. Therefore, we improved the model and analysis settings. In order to get a good match, we took the following actions. The dummy satellite was updated by refining the mesh. The jig was more precisely modeled to represent the experiment. The connections between panels were modified with point connections.

Because there are several resonant frequencies involved, to compare the analysis and the experiment, we divided the frequencies into three regions: below 100 Hz, 100 to 200 Hz, and above 200 Hz. The peak value among each frequency range and its location is listed at 18 measurement points on the internal panels of the dummy satellite. In the table, the errors are defined by dividing the absolute value of the difference between the experiment and the analysis by the experimental value. The frequency increment of the analysis was matched to the frequency interval of the experimental PSD, i.e. 5 Hz. The comparisons between analysis and experiments show good agreement for the 20 to 100 Hz region of the dummy satellite. The average error is less than 17% and the resonant frequency differs only by 3.5%. The agreement degrades with higher frequency. However, the error is 30% in the AF and 7% in the resonant frequency. Table 4 lists the average error of all three directions of vibration excitation. Overall, the accuracy of the analysis is good enough for the present purpose.

Table 1. Comparison of amplification factor and resonant frequency (20-100 Hz).

Units	Experiment		Analysis		Error	
	AF	Resonant Frequency (Hz)	AF	Resonant Frequency (Hz)	AF	Resonant Frequency
DM1	6.3	45	6.5	45	0.032	0.000
PCU	2.6	45	2.9	45	0.115	0.000
Battery	7.6	45	8.2	45	0.079	0.000
+x center	5.2	45	6.2	45	0.192	0.000
DM6	7.4	40	6.2	45	0.162	0.125
OBC	2.1	40	2.9	40	0.381	0.000
RF	5.9	40	7.5	45	0.271	0.125
+y center	4.3	40	3.8	40	0.116	0.000
DM4	7.7	40	6.4	40	0.169	0.000
DM2	3.6	40	3.0	40	0.167	0.000
DM5	7.9	40	6.1	45	0.228	0.125
-x center	4.3	40	3.9	40	0.093	0.000
DM3	4.2	40	3.8	40	0.095	0.000
DM9	9.3	40	7.4	45	0.204	0.125
DM7	9.6	40	6.6	40	0.313	0.000
DM10	9.1	40	7.1	40	0.220	0.000
-y center	4.8	40	4.1	40	0.146	0.000
DM8	4.0	40	4.1	45	0.025	0.125
Average					0.167	0.035

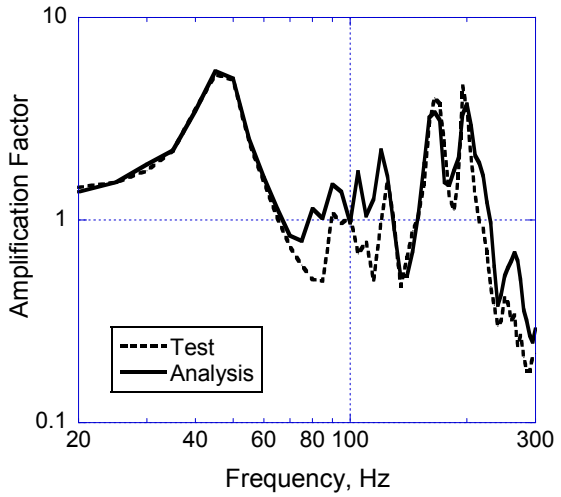

Fig. 8. Example of test and analysis result comparison (horizontal direction).

Table 2. Comparison of amplification factor and resonant frequency (100-200 Hz).

Units	Experiment		Analysis		Error	
	AF	Resonant Frequency (Hz)	AF	Resonant Frequency (Hz)	AF	Resonant Frequency
DM1	1.9	105	1.1	105	0.421	0.000
PCU	0.8	105	0.6	140	0.250	0.333
Battery	1.0	105	0.6	105	0.400	0.000
+x center	1.2	105	0.7	110	0.417	0.048
DM6	4.9	105	2.7	110	0.449	0.048
OBC	2.3	195	2.2	195	0.043	0.000
RF	2.5	195	3.8	170	0.520	0.128
+y center	1.3	200	1.4	200	0.077	0.000
DM4	1.0	185	0.8	200	0.200	0.081
DM2	0.9	105	0.7	105	0.222	0.000
DM5	1.3	185	0.8	160	0.385	0.135
-x center	0.7	190	0.5	190	0.286	0.000
DM3	1.1	195	0.9	200	0.182	0.026
DM9	5.1	105	2.7	140	0.471	0.333
DM7	3.1	105	1.8	110	0.419	0.048
DM10	9.2	105	4.9	110	0.467	0.048
-y center	0.6	195	0.7	200	0.167	0.026
DM8	3.8	195	3.1	200	0.184	0.026
Average					0.309	0.071

Table 3. Comparison of amplification factor and resonant frequency (200-300 Hz).

Units	Experiment		Analysis		Error	
	AF	Resonant Frequency (Hz)	AF	Resonant Frequency (Hz)	AF	Resonant Frequency
DM1	1.3	280	0.9	275	0.308	0.018
PCU	1.4	275	1.6	300	0.143	0.091
Battery	0.9	280	0.8	300	0.111	0.071
+x center	1.5	250	1.0	260	0.333	0.040
DM6	2.1	215	1.7	220	0.190	0.023
OBC	9.3	300	5.0	260	0.462	0.133
RF	5.5	240	2.9	245	0.473	0.021
+y center	2.8	240	1.6	255	0.429	0.063
DM4	1.2	230	0.8	235	0.333	0.022
DM2	1.0	250	0.9	225	0.100	0.100
DM5	1.6	230	1.4	245	0.125	0.065
-x center	1.3	295	1.1	225	0.154	0.237
DM3	1.3	245	1.2	240	0.077	0.020
DM9	1.3	250	0.9	255	0.308	0.020
DM7	1.2	245	0.9	255	0.250	0.041
DM10	2.3	260	1.5	280	0.348	0.077
-y center	0.5	280	0.8	250	0.600	0.107
DM8	4.7	205	2.9	220	0.383	0.073
Average					0.285	0.068

Table 4. Average error of analysis. Vertical direction = y axis.

Excitation direction	20~100 Hz		100~200 Hz		200~300 Hz	
	AF	Freq.	AF	Freq.	AF	Freq.
x	0.167	0.035	0.309	0.071	0.285	0.068
y	0.206	0.003	0.205	0.152	0.332	0.036
z	0.241	0.021	0.244	0.107	0.446	0.118

3. Extrapolation to Other Structure Types

The purpose of the FE analysis is to extend and extrapolate from the experimental result. On the other hand, we try to accumulate more data from other satellites to improve the satellite-to-satellite variation or gather the data based on numerical analysis. In this section, we present a review of the steps involved in FE analysis of vibration acceleration distribution in the dummy satellite structures and other types of 50-cm-class satellite models, such as T-type and Pi-type structures.

After verifying the accuracy of the analysis software and the modeling, we now extend the object of study to other structural types. The dummy satellites studied in the experiment were of the Yojo-han type. Schematic pictures of each structural type are shown in Fig. 9. A summary of the FE model of each structural type is listed in Table 5. Virtual sensors were attached to the internal panels.

Table 5. Summary of the dummy satellite FE model.

Subject	Structural type		
	Yojo-han type	T-type	Pi-Type
Dimension	50 cm x 50 cm x 50cm		
Total weight	50 kg		
Number of virtual sensors	18	8	8
Number of nodes	80,051	64,684	74,518
Number of elements	48,381	40,176	44,199

A linear random vibration analysis was done on the three structural models. The analysis was carried out only in the frequency range from 20 to 300 Hz. We further divided the frequency ranges into three zones: 20 to 100, 100 to 200, and 200 to 300 Hz. Figures 10 and 11 show the results from the

T-type structure for horizontal and vertical vibration direction, respectively.

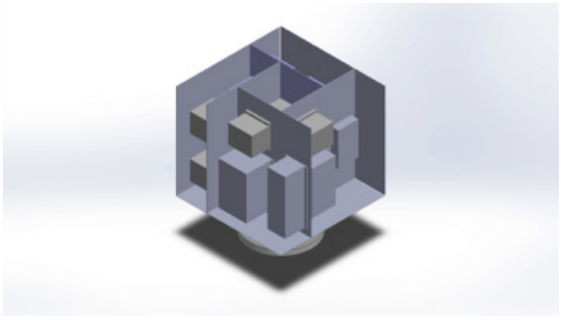

a) Yojo-han structure

b) Pi-type structure

c) T-type structure

Fig. 9. Basic types of micro/nanosatellite structures.

In the Appendix, we list the results from the sensors of all three types. Using the tables in the appendix, we now derive the lower and upper limits of the AF and the resonant frequencies. To do so, we assume that the values of the AF at different locations follow a log-normal distribution[3]. Then, variable y is defined by

$$y = \log_{10} x \quad , \tag{1}$$

where x is the AF at each point following a normal distribution. Then the normal tolerance limits (NTL) of the peak AFs are computed for the transformed predictions using

$$\mathrm{NTL}_y(\mathrm{n}, \beta, \gamma) = \bar{y} \pm k_{n,\beta,\gamma} \; s_y \tag{2}$$

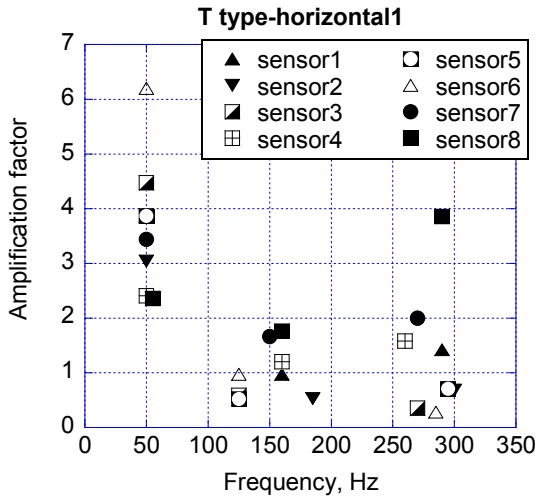

Fig. 10. Peak amplification factor and resonant frequency (T-type, horizontal excitation).

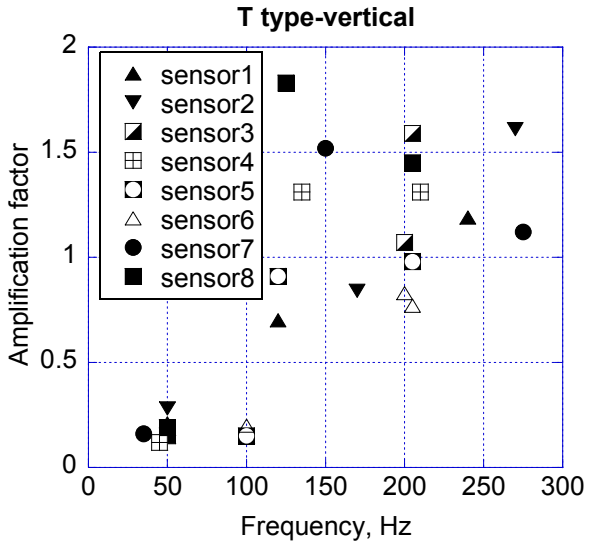

Fig. 11. Peak amplification factor and resonant frequency (T-type, vertical excitation).

The NTL is defined as the value y that will exceed at least β portion of all possible values of y with a confidence coefficient of γ, and is given by Ref. 2). In Eq. (2), the term $k_{n,\beta,\gamma}$ is called the normal tolerance factor, and is a tabulated value which depends on the values of n, β, and γ. For the Yojo-han type, n=18. For the T- and Pi- types, n=8. The NTL was chosen as 95/50 (β=0.95, γ=0.50). Then the factor $k_{n,\beta,\gamma}$ is 1.67 for the Yojo-han and 1.72 for the T- and Pi- types.

For the resonant frequencies, we used a normal distribution and calculated the NTLs. The NTLs of the three structural types are listed in Tables 6, 7 and 8. In those tables, one frequency range of 20 to 300 Hz is used, instead of three subdivisions.

Table 6. Resonant frequency range of the Yojo-han type.

	Resonant frequency [Hz]		
	X (horizontal)	Z (horizontal)	Y (vertical)
Average	42.5	41.9	135.6
Standard deviation	2.6	2.5	10.3
Lower value	38.2	**37.8**	**118.4**
Upper value	46.8	**46.1**	**152.7**

Table 7. Resonant frequency range of the T-type.

	Resonant frequency [Hz]		
	X (horizontal)	Z (horizontal)	Y (vertical)
Average	50.6	51.9	200.6
Standard deviation	1.8	2.6	45.9
Lower value	**47.6**	47.4	**121.6**
Upper value	**53.7**	56.3	**279.6**

Table 8. Resonant frequency range of the Pi type.

	Resonant frequency [Hz]		
	X (horizontal)	Z (horizontal)	Y (vertical)
Average	50.0	54.4	237.5
Standard deviation	0.0	1.8	2.7
Lower value	**50.0**	51.3	**232.9**
Upper value	**50.0**	57.4	**242.1**

Tables 9-11 show the NTL of the AF for each satellite structure. To deduce the NTL, we used the same method as with the experimental data.[3)]

Table 9. NTL of amplification factor (Yojo-han, 20-300 Hz, log values are shown in parentheses).

	Amplification Factor		
	X (horizontal)	Z (horizontal)	Y (vertical)
Average	5.1(0.71)	4.8(0.68)	3.3(0.52)
Standard deviation	1.4(0.16)	1.2(0.09)	1.1(0.05)
NTL (Min)	2.8(0.45)	**3.4(0.53)**	**2.7(0.43)**
NTL (Max)	9.2(0.96)	6.8(0.83)	4.0(0.60)

Table 10. NTL of amplification factor (T-type, 20-300 Hz, log values are shown in parentheses).

	Amplification factor		
	X (horizontal)	Z (horizontal)	Y (vertical)
Average	3.5(0.55)	2.4(0.38)	1.3(0.12)
Standard deviation	1.4(0.14)	1.7(0.22)	1.3(0.12)
NTL (Min)	**2.0(0.31)**	1.0(-0.01)	**0.8(-0.08)**
NTL (Max)	6.1(0.79)	5.8(0.76)	2.1(0.32)

Table 11. NTL of amplification factor (Pi type, 20-300 Hz, log values are shown in parentheses).

	Amplification Factor		
	X (horizontal)	Z (horizontal)	Y (vertical)
Average	1.9(0.28)	1.4(0.15)	4.8(0.68)
Standard deviation	1.2(0.07)	1.5(0.18)	1.8(0.25)
NTL (Min)	**1.4(0.16)**	0.7(-0.16)	**1.8(0.26)**
NTL (Max)	2.6(0.41)	2.8(0.45)	12.7(1.10)

4. Derivation of the Unit QT Level

We now compare the unit QT level to be derived from the analytical results and the one already previously proposed based on the experimental data (Fig. 1). To derive the unit QT level, we use the same methodology described in Ref. 3. For the T-type structure, between 48 and 54 Hz, we chose an AF of 2.0. Between 122 and 280 Hz, we chose an AF of 1.0. An AF of 0.8 was not chosen. We set 1.0 as the minimum instead. We chose a maximum number at the lower limit because the test level we are trying to propose is to guarantee a minimum level of assurance. Unit manufacturers have no way of knowing in which direction their products will be mounted in the satellite. It could be on the plane perpendicular to the thrust axis or on the plane parallel to the thrust axis. At least it is possible that the product will undergo vibration amplified by a factor of 2.0 in one direction. Between the frequencies of 54 and 122 Hz or 20 and 48 Hz, we extrapolate the peak values, assuming a single-degree-of-freedom vibration system with a Q-value, typically Q=5.

For the Pi-type structure, the unit QT level is 1.4 at 50 Hz and 1.8 between 233 and 242 Hz. The unit QT level is derived by multiplying the acceptance vibration levels of various launchers by the AFs. In Table 12, we summarize the selected values.

Figure 12 shows the AFs in the frequency ranges from 20 to 2000 Hz derived from the experiments.[3)] It should be noted that at low frequencies, less than 300 Hz, the experimental data used were only those measured at the top corners. Instead of using the measurement data inside the dummy satellite, the external corner point data was used to increase the variety of the satellite types. Therefore, the peak AF of 4.2 between 31 and 76 Hz derived from the experimental data of seven satellites may be an overestimate of the AF. Although it may be an overestimate, considering the average error of 24% in the analysis below 100 Hz (see Table 4), we keep the number 4.2 to be conservative. For simplicity, we also use 4.2 between 20 and 31 Hz.

For the frequency range between 118 and 153 Hz, the analysis of the Yojo-han-type structure shows an AF of 2.7. It is almost the same as the AF of 2.6 derived from the experimental data from seven satellites. Considering a numerical error of 30% between 100 and 200 Hz (see Table 4), however, the factor of 2.7 derived from the analysis may be as large as 3.5. Therefore, for the frequency range between 118 and 153 Hz, we use a factor of 3.5 instead of 2.7. For a frequency above 153 Hz, the AF of 3.5 is varied, assuming a single-degree-of-freedom transmission factor, until it reaches 2.6 (see Ref. 3)). This occurs at 165 Hz. Beyond that, the AF is 2.6 until 214 Hz. The Pi-type structure gives an AF of 1.8 between 233 and 242 Hz. Considering a numerical error as large as 45%, we use a factor of 2.6 between 233 and 242 Hz. For frequencies above 242 Hz, the AF is unchanged.

Table 13 lists the AF and range of resonant frequency, taking into account the newly obtained results. Figure 13 plots the AF from 20 to 2000 Hz after connecting the six resonant

frequency zones.

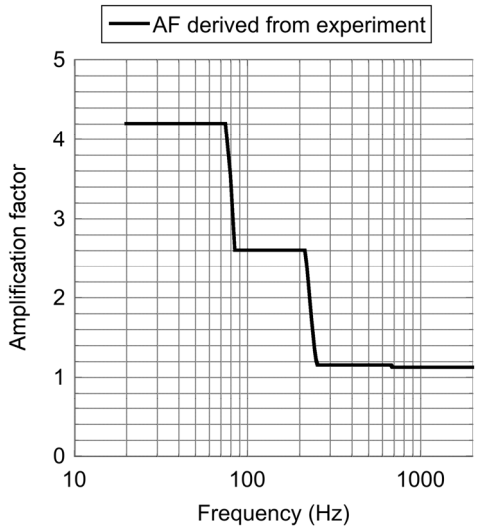

Fig. 12. Amplification factor for unit QT test levels derived by the experiments.[3)]

Table 12. Peak amplification factor and resonant frequencies to be used for unit QT level derivation. Underlined values were used to derive the unit QT level shown in Fig. 1.

	Horizontal		Vertical	
	Resonant frequency (horizontal) [Hz]	Peak AF	Resonant frequency (vertical) [Hz]	Peak AF
Experiment (Statistics of seven satellites using the sensor at the top corner)	31~76	4.2	130~214	2.6
Experiment (Yojo-han, i.e., dummy satellite; statistics of the internal sensors)	20-89.7 453~677 1439-2000	2.9 1.15 1.12	20-302.1 255-384 1450-1933	2.4 1 1
Analysis (Yojo-han; statistics of the internal sensors)	38-46	3.4	118-153	2.7
Analysis (T-type; statistics of the internal sensors)	48-54	2.0	122-280	1.0
Analysis (Pi-type; statistics of the internal sensors)	50	1.4	233-242	1.8

Table 13. Peak amplification factor and frequencies to be used for unit QT level derivation.

Resonant frequency range (Hz)	AF
20~76	4.2
118~153	3.5
165~214	2.6
233~242	2.6
453~677	1.15
1439-2000	1.12

We now plot the Power Spectrum Density (PSD) for the random vibration test. Figure 14 plots the PSD obtained by multiplying the values in Fig. 13 by a PSD provided by a rocket. Figure 14 also plots the PSD to be proposed as an ISO test level obtained by smoothing the former. The newly proposed one is slightly different from that shown in Fig. 1. It is flat at 0.29 (G^2/Hz) between 105 and 165 Hz. Below 105 Hz, there is a straight line starting from 0.057 (G^2/Hz) at 20 Hz. Above 165 Hz, there is another straight line to 0.040 (G^2/Hz) at 2000 Hz. The RMS values are both 13.8 Grms.

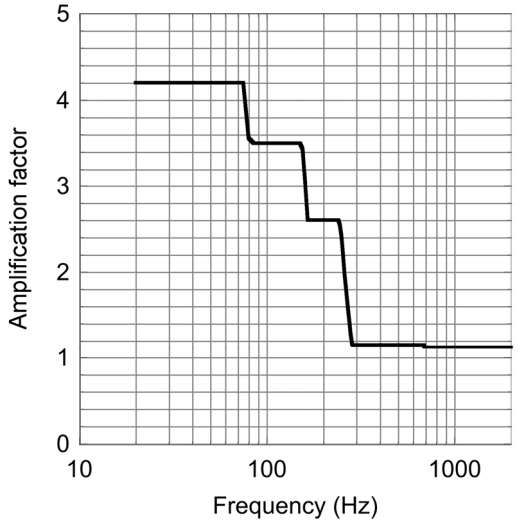

Fig. 13. Amplification factor for unit QT test levels derived by the experiments and analysis.

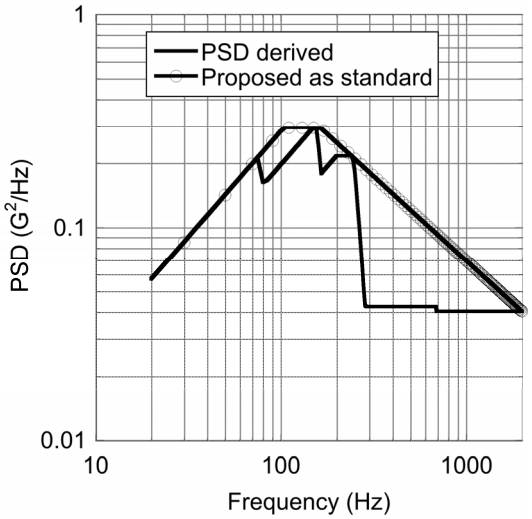

Fig. 14. Newly proposed PSD for unit QT random vibration.

The PSD in Fig. 14 is higher than PSD in Fig.1 between 80 and 150 Hz. The reason is clear by comparing Figs. 12 and 13. Previously we used AF of 2.6 at around 100 Hz based on the experimental data values measured at the external corner of satellites. This time, we used AF of 3.5 based on the analysis of data values obtained at the internal sensors. The AF value of 3.5 was obtained by multiplying the value of 2.7 in the row "Analysis (Yojo-han; statistics of the internal sensors)" in Table 12, considering a numerical error of 30% between 100 and 200 Hz (see Table 4). Because Fig. 14 shows the unit QT test levels to be applied for internal units, it is more reasonable

to use the values obtained from the internal sensors.

5. Conclusion

We aimed to propose a random vibration test level that gives a minimum guarantee that a unit sold as "a satellite unit" has a certain level of tolerance against the space environment. In order to determine the unit QT level, a series of random vibration tests were conducted up to 2,000 Hz. The test data of seven 50-cm-class microsatellites were also collected. Based on the statistical analysis, a random vibration test level was proposed and included in a new ISO draft.

In order to cover a wider range of structures expected in micro/nanosatellites, structural analysis was carried out using FE analysis software. In the analysis, the acceleration inside various types of satellites, i.e., Yojo-han, T-type and Pi-type, was calculated. The results have been used to update the unit QT level. A slight change has been made to the previously proposed unit QT test level.

The Kyushu Institute of Technology is serving as a test center for Japanese micro/nanosatellites. We accumulate the experimental data of various types of micro/nanosatellites. The experimental database should be constantly revised to improve the accuracy of the statistics.

Appendix: Results of Analysis

Table 14. Peak amplification factor and resonant frequency statistics of Yojo-han-type structure (X-direction, horizontal**1**).

	20-100 Hz		100-200 Hz		200-300 Hz	
	AF	Resonant Frequency (Hz)	AF	Resonant Frequency (Hz)	AF	Resonant Frequency (Hz)
DM1	6.5	45	1.1	105	0.9	275
PCU	2.9	45	0.6	140	1.6	300
Battery	8.2	45	0.6	105	0.8	300
+x center	6.2	45	0.7	110	1.0	260
DM6	6.2	45	2.7	110	1.7	220
OBC	2.9	40	2.2	195	5.0	260
RF	7.5	45	3.8	170	2.9	245
+y center	3.8	40	1.4	200	1.6	255
DM4	6.4	40	0.8	200	0.8	235
DM2	3.0	40	0.7	105	0.9	225
DM5	6.1	45	0.8	160	1.4	245
-x center	3.9	40	0.5	190	1.1	225
DM3	3.8	40	0.9	200	1.2	240
DM9	7.4	45	2.7	140	0.9	255
DM7	6.6	40	1.8	110	0.9	255
DM10	7.1	40	4.9	110	1.5	280
-y center	4.1	40	0.7	200	0.8	250
DM8	4.1	45	3.1	200	2.9	220

References

1) Bouwmeester, J. and Guo, J.: Survey of Worldwide Pico- and Nanosatellite Missions, Distributions and Subsystem Technology, *Acta Astronautica,* **67** (2010), pp. 854–862.
2) Cho, M., Date, K., Horii, S. and Obata, S.: Introduction of Nanosatellite Environment Test Standardization (NETS) Project, Background and Objectives, *Proceedings of Joint-Conference on Space Technology and Science*, JSASS-2011-4424, 2011.
3) Dynamic Environmental Criteria, NASA-HDBK-7005, 2001.
4) Batsuren, A., Tomida, K., Hatamura, T., Masui, H. and Cho, M.: Laboratory Tests to Standardize Environment Test Conditions of Micro/Nano Satellite Units, *Trans JSASS Aerospace Tech Japan,* **12** (2014), pp. Pf_1-Pf_10,.
5) Batsuren, A., Tomida, K., Hatamura, T., Masui, H. and Cho, M.: Erratum to "Laboratory Tests to Standardize Environment Test Conditions of Micro/Nano Satellite Units" *Trans. JSASS Aerospace Tech. Japan,* **12**(2014), pp. Pf_1-Pf_10.
6) Tomida, K., Batsuren, A., Hatamura, T., Masui, H. and Cho, M.: Basic Research on Vibration Test Level for Nanosatellite Components, *Proceedings of 29th International Symposium on Space Technology and Science*, 2013-f-26, 2013.

Table 15. Peak amplification factor and resonant frequency statistics of Yojo-han-type structure (Z-direction, horizontal**2**).

	20-100 Hz		100-200 Hz		200-300 Hz	
	AF	Resonant Frequency (Hz)	AF	Resonant Frequency (Hz)	AF	Resonant Frequency (Hz)
DM1	5.43	45	3.74	195	2.91	205
PCU	4.05	45	6.88	200	5.48	205
Battery	5.6	45	2.82	195	5.27	260
+x center	3.48	45	2.5	200	2.14	205
DM6	5.09	45	1.02	190	0.6	205
OBC	3.18	40	1.24	200	1.3	260
RF	4.98	45	0.65	115	0.47	255
+y center	4.48	45	0.69	115	0.49	210
DM4	6.55	40	3.52	180	2.76	205
DM2	5.08	40	8.76	110	1.56	250
DM5	6.76	40	6.29	120	3.01	205
-x center	4.19	40	1.01	175	0.82	205
DM3	4.3	40	3.3	105	3.27	205
DM9	5.58	40	0.82	120	0.49	235
DM7	5.6	40	1.02	150	1.05	275
DM10	5.91	40	1.06	115	0.57	235
-y center	4.35	40	0.57	105	0.87	260
DM8	3.82	40	0.79	145	1.87	240

Table 16. Peak amplification and resonant frequency statistics of Yojo-han-type structure (Y-direction, vertical).

	20-100 Hz		100-200 Hz		200-300 Hz	
	AF	Resonant Frequency (Hz)	AF	Resonant Frequency (Hz)	AF	Resonant Frequency (Hz)
DM1	2.03	90	3.08	125	2.00	245
PCU	1.57	90	3.25	145	1.51	215
Battery	1.53	95	3.72	140	2.25	250
+x center	1.51	90	3.24	140	2.32	245
DM6	2.68	90	2.6	125	1.26	230
OBC	2.21	90	2.9	125	1.65	230
RF	2.35	90	3.03	155	1.59	215
+y center	2.19	90	2.73	155	1.62	230
DM4	1.92	90	3.48	140	1.24	260
DM2	2.61	85	3.6	140	1.23	260
DM5	1.9	90	3.83	140	1.43	260
-x center	2.07	85	3.36	140	1.33	260
DM3	2.21	90	3.51	140	1.88	250
DM9	2.41	95	3.34	125	1.27	265
DM7	2.38	80	3.44	125	1.27	225
DM10	2.31	95	2.82	130	1.28	230
-y center	1.93	80	3.48	125	1.31	260
DM8	1.99	95	3.88	125	1.03	270

Table 17. Peak amplification factor and resonant frequency statistics of T-type structure (X-direction, horizontal**1**).

	20-100 Hz		100-200 Hz		200-300 Hz	
	AF	Resonant frequency [Hz]	AF	Resonant frequency [Hz]	AF	Resonant frequency [Hz]
Sensor1	3.86	50	0.97	160	1.42	290
Sensor2	3.04	50	0.53	185	0.68	300
Sensor3	4.47	50	0.59	125	0.35	270
Sensor4	2.41	50	1.2	160	1.58	260
Sensor5	3.87	50	0.52	125	0.71	295
Sensor6	6.2	50	0.97	125	0.28	285
Sensor7	3.44	50	1.66	150	2	270
Sensor8	2.36	55	1.76	160	3.86	290

Table 18. Peak amplification factor and resonant frequency statistics of T-type structure (Z-direction, horizontal**2**)

	20-100 Hz		100-200 Hz		200-300 Hz	
	AF	Resonant frequency [Hz]	AF	Resonant frequency [Hz]	AF	Resonant frequency [Hz]
Sensor1	2.34	50	1.04	180	1.9	300
Sensor2	2.03	50	1.62	200	1.91	205
Sensor3	3.07	50	1.06	200	1.99	275
Sensor4	1.24	50	1	180	1.66	300
Sensor5	3.42	55	2.05	200	2.33	205
Sensor6	4.2	55	1.27	185	2.43	270
Sensor7	1.05	55	0.63	200	0.87	210
Sensor8	3.81	50	0.55	170	0.58	280

Table 19. Peak amplification factor and resonant frequency statistics of T-type structure (Y-direction, vertical).

	20-100 Hz		100-200 Hz		200-300 Hz	
	AF	Resonant frequency [Hz]	AF	Resonant frequency [Hz]	AF	Resonant frequency [Hz]
Sensor1	0.21	50	0.7	120	1.19	240
Sensor2	0.28	50	0.84	170	1.61	270
Sensor3	0.15	50	1.07	200	1.59	205
Sensor4	0.12	45	1.31	135	1.31	210
Sensor5	0.15	100	0.91	120	0.98	205
Sensor6	0.2	100	0.83	200	0.77	205
Sensor7	0.16	35	1.52	150	1.12	275
Sensor8	0.19	50	1.83	125	1.45	205

Table 20. Peak amplification factor and resonant frequency statistics of Pi-type structure (X-direction, horizontal**1**).

	20-100 Hz		100-200 Hz		200-300 Hz	
	AF	Resonant frequency [Hz]	AF	Resonant frequency [Hz]	AF	Resonant frequency [Hz]
Sensor1	2.13	50	0.15	190	0.68	255
Sensor2	1.63	50	0.11	155	0.79	290
Sensor3	1.81	50	0.22	185	0.72	295
Sensor4	2.00	50	0.21	185	0.98	255
Sensor5	2.40	50	0.15	145	1.13	255
Sensor6	2.11	50	0.15	190	0.61	280
Sensor7	2.03	50	0.20	190	0.61	260
Sensor8	1.42	50	0.18	190	0.42	260

Table 21. Peak amplification factor and resonant frequency statistics of Pi-type structure (Z-direction, horizontal**2**).

	20-100 Hz		100-200 Hz		200-300 Hz	
	AF	Resonant frequency [Hz]	AF	Resonant frequency [Hz]	AF	Resonant frequency [Hz]
Sensor1	1.55	55	0.2	200	0.18	300
Sensor2	1.88	55	0.14	170	0.19	300
Sensor3	2.05	55	0.14	115	0.08	300
Sensor4	1.25	55	0.38	190	0.64	300
Sensor5	0.79	55	0.42	190	0.63	300
Sensor6	1.45	55	0.18	120	0.13	300
Sensor7	2.29	50	0.29	200	1.06	240
Sensor8	0.78	55	0.19	165	0.16	300

Table 22. Peak amplification factor and resonant frequency statistics of Pi-type structure (Y-direction, vertical).

	20-100Hz		100-200Hz		200-300Hz	
	AF	Resonant frequency[Hz]	AF	Resonant frequency [Hz]	AF	Resonant frequency[Hz]
Sensor1	1.32	100	6.3	190	11	240
Sensor2	1.21	100	4.31	190	6.34	240
Sensor3	0.82	100	1.86	190	2.87	240
Sensor4	0.5	100	0.92	190	2.69	235
Sensor5	0.8	100	1.52	190	2.54	235
Sensor6	1.14	100	2.21	185	3.62	235
Sensor7	1.17	100	2.92	190	6.64	235
Sensor8	1.23	100	4.29	190	8.27	240